Combined analysis of the time-resolved transcriptome and proteome of the pathogenicity-activated plant pathogen *Xanthomonas oryzae* pv. *oryzae*

Seunghwan Kim[1], Wooyoung Eric Jang[2], Min-Sik Kim[2, 3§], Jeong-Gu Kim[1§], Lin-Woo Kang[4§]

[1]Genomics Division, National Academy of Agricultural Sciences (NAAS), Rural Development Administration (RDA), Jeonju 54874, Republic of Korea; [2]Department of Applied Chemistry, Kyung Hee University, Yongin 17104, Republic of Korea; [3]Department of New Biology, DGIST, Daegu 42988, Republic of Korea; [4]Department of Biological Sciences, Konkuk University, 1 Hwayang dong, Gwangjin-gu, Seoul 05029, Republic of Korea

[§]Corresponding authors:

Dr. Lin-Woo Kang

Department of Biological Sciences, Konkuk University, Seoul 05029, Republic of Korea; Tel. 82-2-450-4090; Fax: 82-2-444-6707; E-mail: lkang@konkuk.ac.kr

Dr. Jeong-Gu Kim

Genomics Division, National Academy of Agricultural Science (NAAS), Rural Development Administration (RDA), Jeonju 54874, Republic of Korea; Tel. 82-63-238-4566; E-mail: jkim5aug@korea.kr

25 Dr. Min-Sik Kim, Department of New Biology, DGIST, Daegu 42988, Republic of Korea; E-

26 mail: mkim@dgist.ac.kr

27

28 Running title: analysis of transcriptome and proteome in P-activated Xoo

29

Abstract

Xanthomonas oryzae pv. *oryzae* (Xoo) is a plant pathogen responsible for causing bacterial blight in rice. It is responsible for blight outbreaks in most rice-producing countries and can reduce the rice yield by 50% due to the lack of an effective pesticide. The immediate alterations in Xoo upon initial contact with rice at the infection site are essential for pathogenesis. Here, we studied time-resolved gene expression in pathogenicity-activated Xoo cells at the transcriptome and proteome levels. The early response genes of Xoo include genes related to cell motility, inorganic ion transport, and effectors, which aid the Xoo cells to invade damaged rice leaf tissues, obtain scarce cofactors, and evade rice immune responses, respectively. Alteration of gene expression is initiated as early as few minutes after the initial interaction and changes with time. Although there was a correlation between the overall expression patterns of mRNAs and proteins for many genes, some genes also exhibited differences with respect to the expression timing and level of mRNAs and proteins, suggesting an important role of translational regulation in the early stages of pathogenesis. Gene expression analysis using time-resolved transcriptome and proteome data provided valuable information regarding Xoo pathogenesis during the initial stages of Xoo-rice interaction and revealed translational regulation of gene expression in bacteria.

Keywords: Xoo-rice interactions, proteome and transcriptome, time-resolved gene expression, *Xanthomonas oryzae* pv. *oryzae*, pathogenicity, translational regulation

Introduction

Rice (*Oryza sativa* L.) is the most widely consumed staple food, sustaining two-thirds of the world's population (Jackson, 2016). Bacterial blight of rice caused by *Xanthomonas oryzae* pv. *oryzae* (Xoo) is a devastating disease for which an effective pesticide has not been developed yet; it is known to cause severe yield losses of up to 50% in several rice-growing countries (Oliva et al., 2019). The demand for rice is expected to increase by at least 25% by 2030, owing to the rapidly growing world population, environmental stress arising in response to climate change, and pathogen pressure (Li et al., 2014). Further, the Green Revolution has resulted in a shift in rice cultivation, from varied traditional landraces to limited high-yielding varieties, via artificial selection. This has resulted in the co-evolution of crop pathogens including Xoo with the selected host races in the modern agricultural ecosystem (Quibod et al., 2020).

The pathogen-host system of Xoo and rice serves as an ideal agricultural model to study crop diseases in a field setting at the molecular level; this is facilitated by the early elucidation of the whole genome structure of both Xoo and rice (Jackson, 2016; Lee et al., 2005). Xoo typically invades rice leaves through the wounds or hydathodes and replicates in the xylem vessels to cause disease (Mew et al., 1993). Rice contains a two-tiered innate immune system, consisting of pathogen-associated molecular pattern- and effector-triggered immunity, which protects against Xoo and initiates the hypersensitivity response at the infection site (Jones and Dangl, 2006). In Xoo-rice interactions, Xoo injects effectors into rice cells to modulate the cellular activities of the host to promote pathogenesis (Tsuge et al., 2014). The early interactions between Xoo and rice at the infection site determine the fate of infection, i.e., occurrence of disease or initiation of the immune response. The environmental conditions prevalent at the site of infection are varied and complex, and our understanding of

alterations in the Xoo cells in response to the initial interactions with rice is limited.

Transcription and translation are tightly coupled in bacteria and can occur simultaneously in the cytosol (Hershey et al., 2019). Although proteins are the final functional products of genes, the quantity of specific mRNA molecules often represents the expression level of a gene at a given time point with the well-established RNA sequencing (RNA-Seq) technology. In comparison, high resolution mass spectrometry-based quantitative proteomics is a more recent analytical technique, and still has a lower coverage of protein products, requires greater sample quantity, and is more expensive (Schubert et al., 2017).

We had previously developed an *in vitro* pathogenicity assay to recapitulate Xoo-rice interactions at the site of infection by treating Xoo cells with the rice homogenate (RLX), and assessed the time-resolved changes in the transcriptome (Kim et al., 2016; Kim et al., 2013; Kim et al., 2011). The *in vitro* pathogenicity assay provides high signal to noise data with Xoo cells synchronized with respect to the timing of pathogenicity activation. Transcriptome data from RNA-Seq experiments revealed that most virulence genes of Xoo were upregulated within an hour of the initial interaction with RLX, and these upregulated genes were related to bacterial motility, inorganic ion transport, hypersensitive response and pathogenicity (*hrp*), bacterial toxins and effectors of avirulence (*avr*), plant cell wall degradation, and extracellular polysaccharide synthesis and secretion (Kim et al., 2016).

Here, we expand the study of the gene expression in pathogenicity-activated (P-activated) Xoo from the transcriptome to the proteome and compare the time-resolved gene expression in terms of both mRNA and protein. The time-dependent expression of mRNAs and proteins and the kinetics of expression in response to the pathogenic signal allow the visualization of the immediate alterations in gene expression profiles in Xoo cells and reveal the timely regulation of bacterial translation.

Results

Time-resolved proteome data

We coupled LC-MS/MS with an *in vitro* assay system to obtain the time-resolved proteome data for P-activated Xoo cells (Scheme 1). The *in vitro* assay system recapitulated the initial interaction between Xoo cells and damaged rice leaf tissues at the site of infection; this was achieved by adding fresh RLX—prepared by grinding the leaves of a Xoo-susceptible rice cultivar (Milyang 23) in liquid nitrogen—to a Xoo cell culture in the mid-exponential phase. Samples for proteome analysis were collected from RLX-treated (P-activated) and untreated (control) Xoo cells at 0, 30, 60, 90, and 120 min after RLX treatment (Table S1).

Analysis on UniProt revealed that the total 4,733 predicted open reading frames in the Xoo genome corresponded to 4,382 proteins in the proteome, of which 2,589 proteins (59%) were identified for at least one time point and 2,296 proteins (52%) were detected in both replicates (Figure S1A). Median sequence coverages for total identified proteins was 23% and 24% for each of the independent duplicate experiments (Figure S1B). A total of 20,963 and 19,684 non-redundant peptides were identified in both replicates, with 47,025 and 41,428 peptide-spectrum matches, respectively (Figure S1C).

Protein abundance values obtained after quantile-normalization (Figure S2A) were used for pairwise comparisons; the Pearson's correlation coefficients corresponding to the abundance values showed close correlations (0.98-0.99), indicating comparable cellular concentration of most proteins (Figure S2B). The smallest correlations were observed for the RLX-treated samples at 30 min, indicating greater changes in the proteome during the initial 30 min; this was consistent with the transcriptome data. We further performed a principal component analysis to determine the relationships between the assessed samples. Figure S2C shows that the P-activated sample at 0 min clustered closely with all control samples, whereas the P-

activated samples at other time points were more spread out. The proteome of the P-activated Xoo cells at 30 min was considerably different from that of P-activated Xoo at other time points; this was consistent with the results of the pairwise multi-scatter plot (Figure S2B).

Time-supervised hierarchical clustering was performed to determine temporal and synchronized changes in protein abundance. Two distinct synchronized patterns—one decreasing and the other increasing in response to RLX treatment—were observed (Figure 1). The two lists including proteins exhibiting the two patterns were used for STRING analysis, which produced two interaction networks (Figure S3A-B). Several genes related to cell motility, inorganic ion transport, and transcriptional regulators were immediately responsive to the pathogenicity signal (Table S2); these have been described in detail in the discussion section.

Up and down regulated proteins

Quantitative proteome data obtained from P-activated and control Xoo cells at every 30 min allowed the visualization of the three-dimensional protein expression data in terms of the genes, time intervals, and expression levels (Figure 1 and Table S3). For all the open reading frames, approximately 93 (2.0%), 213 (4.5%), and 468 (9.9%) proteins were upregulated by more than 200% (2-fold), 50%, and 20% at 30 min, respectively, and approximately 7 (0.1%), 93 (2.0%), and 561 (11.9%) proteins were downregulated to less than 25% (2-fold), 50%, and 80% at 30 min, respectively (Table S4). Comparable numbers of proteins were up- and downregulated from 30 to 120 min.

In case of the duration of protein expression in P-activated Xoo, 8 (0.2%), 32 (0.7%), and 75 (1.6%) proteins were upregulated for 120 min by more than 200% (2-fold), 50%, and 20%, respectively and 0 (0%), 1 (0.02%), and 87 (1.8%) proteins were downregulated for 120 min

148 to less than 25% (2-fold), 50%, and 80% , respectively (Table S5), indicating that most
149 proteins were temporarily up- or downregulated in the *in vitro* assay.

150 The proteins expressed at 30 min presented the highest change within 120 min. More than
151 90 proteins (1.9%) were upregulated by more than 2-fold at 30 min in each dataset, whereas
152 27 proteins were upregulated in both datasets from the duplicate experiments (Table S6).
153 Almost half of the 27 upregulated proteins were related to cell motility and ion uptake, seven
154 were related to chemotaxis and motility, and five were related to transporters and pumps. In
155 the proteome datasets at 30 min, 95 proteins were downregulated by more than 50%, 17
156 proteins were downregulated in both datasets (Table S7), including transcription-related
157 proteins—such as sigma-54 modulation protein and MetE/MetH family transcriptional
158 regulator—and cell division- and cell cycle-related proteins.
159
160 **Proteome and Clusters of Orthologous Groups (COGs)**
161 To study the global gene expression pattern based on gene function, we superimposed
162 time-dependent protein expression levels as per the functional categories in the Clusters of
163 Orthologous Groups (COG) database (Figure 2), which were grouped into three classes (red,
164 yellow, and blue) depending on the observed pattern. To facilitate the comparison of time-
165 dependent protein expression levels, the expression level at 0 min was set as the reference
166 level (=1) for each gene, and the fold change in the protein expression level was calculated at
167 each time point, as in case of the RNA-Seq data analysis (Kim et al., 2016).
168 The most prominent changes in protein expression in Xoo cells were observed for proteins
169 associated with cell motility (N) and inorganic ion transport and metabolism (P), which were
170 placed in the red class. In category N, two major expression peaks, indicating >2-fold up-
171 regulation, were detected at 30 and 90 min. In category P, upregulated proteins peaked at

around 30 min. Proteins grouped in the yellow class exhibited moderate changes in their expression level, and were divided into nine functional categories, including signal transduction (T), intracellular trafficking, secretion, and vesicular transport (U), energy production and conversion (C), transcription (K), and cell wall/membrane/envelop biogenesis (O). The blue class included proteins associated with other nine categories, the expression levels of which exhibited little or no change when compared with those at 0 min, albeit except for a few proteins.

Comparison of mRNA and protein levels

We compared mRNA and protein levels of each gene in the transcriptome and proteome (Figure 3; thin dashed red lines and solid and dashed thick black lines, respectively). Both transcriptome and proteome data were obtained for up to 2 h (120 min) after RLX treatment. The experimental procedure used to prepare protein samples for LS-MS/MS required at least 30 min, whereas that for mRNA samples required at least 5 min; the time interval for the proteome data was set to 30 min, whereas that for transcriptome data was set to 5-30 min. Due to the different sampling times, the transcriptome data included mRNA levels at additional time points of 5, 10, 15, and 45 min, whereas the proteome data did not include protein levels before 30 min, in which case the protein levels (dashed black lines) were extrapolated based on the protein levels at other time points using non-linear regression.

Flagella and chemotaxis-related genes

Flagella and chemotaxis-related genes encode more than 40 proteins, including structural components and assembly factors of flagellar hook-basal body and filament and chemotaxis proteins (Mukherjee and Kearns, 2014). Two dominant hierarchical clusters, with distinct

196 synchronized patterns of increasing and decreasing proteome concentration (indicated by red
197 and blue, respectively), were identified (Figure 1). The red (359 proteins) and blue (391
198 proteins) clusters included 21 (53%) of the 40 genes related to the flagellar assembly pathway,
199 of which 20 genes were included in the red cluster and the remaining gene was included in
200 the blue cluster (Table S2).

201 We grouped the flagella and chemotaxis-related genes into three gene clusters, i.e., groups
202 I-A, I-B, and II, based on their positions in the genome (Figure 4A). Genes in cluster I-A and
203 I-B were associated with flagellar machinery, such as flagellar basal body hook and type III
204 secretion system (T3SS), whereas cluster II included chemotaxis-related genes.

205 Superimposition of transcriptome and proteome data revealed clearly superimposed peaks
206 of the main upregulated genes in both data at 30 min (Figure 3A). The transcriptome data
207 revealed that most flagella and chemotaxis-related genes were regulated in a similar pattern,
208 i.e., genes in clusters I-A, I-B, and II were downregulated at 5 min and upregulated at 30 min.
209 However, the proteome data presented a different expression pattern. Proteins in clusters I-A
210 and I-B were upregulated at 30 min, consistent with the transcriptome data. However,
211 proteins in cluster II were upregulated at 90 min, exhibiting a delay of 1 h when compared
212 with the transcriptome data (Figure S4).

213

214 *Inorganic ion transport and metabolism genes*

215 Iron uptake genes play a key role in pathogenicity during the early stages of host-pathogen
216 interactions (Garau et al., 2004). TonB-dependent receptors (TBDRs) are bacterial outer
217 membrane proteins that bind and transport ferric chelates of siderophores. Several annotated
218 TBDR genes have been identified in the Xoo KACC10331 genome, including *IroN*, *FyuA*,
219 *FecA*, *BtuB*, *FhuA*, *CirA*, and *FepA* (Kim et al., 2016). Of these, *FecA* (*Xoo0901*) and *CirA*

(*Xoo3793*) were upregulated and *IroN* genes (*Xoo0394* and *Xoo1784*) were downregulated in the transcriptome as well as in the proteome data. In the proteome data, *FecA* (*Xoo0901*) and *CirA* (*Xoo3793*) upregulation peaked at 30 min (Figure 5A). *IroN* genes that were downregulated at the transcript level were also downregulated—or expressed at the same level—at the protein level (Figure 5B). The expression levels of other paralogs of *FecA* and *CirA* genes were comparable with those in the control in the transcriptome as well as the proteome data (Figure S5), indicating that these genes respond to different pathogenic signals—which were missing in the *in vitro* system—or are pseudogenes.

Phosphate uptake genes, i.e., *OprO*, *PhoX*, *PstSCAB*, and *PhoU*, were upregulated in the transcriptome (up to 16-fold) at 5-10 min. The proteome data of OprO, PhoX, PstSCAB, and PhoU revealed 2-3-fold upregulation at 30 min (Figure S6).

Expression and secretion of effectors

In *Xanthomonas oryzae* pv. *oryzicola*, AvrBs2 suppresses host immunity and promotes disease development (Ullah et al., 1998). In *Xanthomonas campestris* pv. *Vesicatoria*, the role of AvrBs3 is that of a transcription activator-like (TAL) effector that activates the expression of plant immunity genes (Kay et al., 2009). The secretion of effectors XoAvrBs2 (*Xoo0168*)—a Xoo ortholog of AvrBs2—and XoAvrBs3 (*Xoo2276*)—a Xoo ortholog of AvrBs3—through T3SS was confirmed upon interaction with RLX (Kim et al., 2013; Kim et al., 2011). In addition to the transcriptome and proteome, the expression and secretion of effectors were assessed using dot blots of Xoo cells transformed with the TAP-tagged effector genes (Figure 6). The expression levels of these factors in the transcriptome and proteome are indicative of their levels within Xoo cells. Dot blots provide information regarding the secreted levels in addition to the cellular levels.

The expression of *XoAvrBs2* transcript was upregulated from 5-30 min, while that of the XoAvrBs2 protein was upregulated at 30 min, as is evident from the transcriptome and proteome data. In the dot blots, the levels of TAP-tagged XoAvrBs2 were upregulated by 4-fold at 5 min and the secretion of XoAvrBs2 was detected as early as 15 min. The expression of *XoAvrBs3* transcript was upregulated and peaked from 5-30 min, whereas that of XoAvrBs3 protein was maintained at almost the same—or slightly lower levels—at 60 min. Dot blots revealed the secretion of XoAvrBs3 from 15 min.

252 **Discussion**

253 Plant pathogens can exhibit complex responses to the initial interactions with the host
254 under varying biotic and abiotic conditions at the site of infection. The immediate response of
255 the plant pathogen under any condition is important for successful infection. In the present
256 study, we analyzed the initial time-dependent responses of Xoo cells in terms of gene
257 expression at both the mRNA and protein levels using an *in vitro* assay system, wherein RLX
258 mimicked the damaged rice leaf tissue. RLX treatment of Xoo culture serves as a baseline for
259 setting the timing of initial interaction between Xoo and RLX; this allows us to study the
260 time-resolved gene expression responses of Xoo cells, with a high signal to noise ratio
261 compared to that of *in vivo* assay systems.

262 Of all the predicted open reading frames in Xoo, we quantified approximately 86% and 49%
263 of the mRNAs and proteins, respectively, in a time-dependent manner. A good
264 correspondence was observed between the mRNA and protein expression of genes. The
265 expression pattern was more synchronized for genes closely located in the genome, (Figure 4
266 and S4); this could be attributed to the polycistronic gene structure in bacteria. With respect
267 to the rapidity of pathogenic gene expression in response to the signals triggered upon
268 interaction with the host, both transcription and translational machineries responded
269 immediately to the interaction, at the earliest assessed time points of 5 and 30 min, and this
270 was reflected in the transcriptome and proteome data (15 min in dot blots). Both mRNAs and
271 proteins presented the greatest variation in their levels during the initial 30 min.

272 The Xoo genes exhibiting the most rapid responses to the initial interaction with RLX,
273 included genes associated with cell motility and inorganic ion uptake, and genes coding for
274 effector molecules. All these three functional categories of genes are closely related to the
275 early stages of pathogenesis. The genes associated with cell motility could be responsible for

the migration and accumulation of the Xoo cells at the site of infection via the damaged xylem tissues or exposed hydathodes in rice. As inorganic ions, such as iron and phosphate ions, function as essential cofactors in all living organisms, bacterial pathogens and host rice cells compete to obtain and secure the limited resources available. Effector molecules are more directly related to pathogenesis and are injected by the Xoo into the rice cells via pili-like T3SS; these molecules modulate the immune system of rice.

The earliest available time-point for comparing the gene expressions in terms of mRNA and protein levels was 30 min after the RLX treatment. At 30 min, 290 mRNAs were upregulated by more than 2-fold in the transcriptome, compared with 93 proteins in the proteome (Table S4), and the average fold change in the expression of the upregulated genes in the transcriptome and proteome was similar, i.e., 3.28- and 3.40-fold, respectively (Table S6). The number of upregulated transcripts is much higher than—even though we figure into our calculations the higher coverage of quantified genes in transcriptome than in proteome—that of the proteins at 30 min, which indicates that not all the upregulated mRNAs are simultaneously translated to proteins.

The difference in the gene expression in terms of the mRNA and protein levels at a given time point suggests the existence of an additional translational regulation step—after transcription—although transcription and translation can occur simultaneously in bacteria. For some genes, the mRNA and protein expression peaks were observed at varying time points. Bacterial pathogenesis appears to involve a fine-tuning mechanism after transcription, which could help adjust the expression of the early-responsive genes under varying biotic and abiotic environmental conditions.

Genes related to flagella and cell motility are clustered in the bacterial genome. In Xoo, three clusters are observed, i.e., I-A, I-B, and II. On superimposing the mRNA and protein

levels in time, the expression of mRNAs and proteins peaked at 30 mins for genes in cluster I, the expression of mRNAs and proteins peaked at 30 and 90 min, respectively, for genes in cluster II. A translational regulation step might be involved that determines the time for the translation of specific mRNAs—coded by flagella and cell motility-related genes—into proteins depending on the priority of each gene.

The hierarchy of the expression of flagella and cell motility-related genes has been extensively studied in the transcriptome of *E. coli*, where sigma and anti-sigma factors are known to be the key transcriptional regulators (Mukherjee and Kearns, 2014). The overall organization of flagella and chemotaxis-related genes is different between *E. coli* and Xoo (Figure S7). In Xoo, the cluster of *fliE-R* genes (cluster I-B) is positioned just downstream to the *flgB-L* genes (cluster I-A), whereas in *E. coli*, chemotaxis genes are present between the two. *flhDC* genes do not have any orthologs in Xoo, and a different transcriptional regulator, i.e., the *fleQ* gene, is present. Based on the nomenclature used in *E. coli*, several Xoo genes classified as Class III genes are located at different positions and their expression regulation is also different. In Xoo, ribosomes or other translation factors might recognize certain unknown priority signals in mRNA transcripts during pathogenesis.

The immediate upregulation of inorganic ion uptake genes, especially iron uptake genes, may aid Xoo cells to obtain the essential cofactor ions, when they are competition with the host cells for nutrition. The iron ion is essential for photosynthesis and respiration and is needed by the redox enzymes; it is an important signaling molecule for pathogenicity. Pathogens commonly use iron chelating molecules or siderophores to derive this scarce inorganic cofactor from the hosts. The leakage of iron ions from damaged leaf tissues might serve as an important signal of infection and might provide an opportunity to secure essential iron ions for the Xoo cells.

In comparison with the flagella and cell motility-related genes that are closely clustered in the genome and exhibit coordinated expression levels, the ion uptake genes are dispersed across the genome and are independently expressed (Figure S8). The separation of these genes facilitates independent regulation. In comparison with the flagella and motility-related genes, the inorganic ion uptake genes exhibited great variation in the mRNA levels but similar protein expression levels (Figure 3).

Effectors are key molecules for pathogenicity that modulate the host immune responses after infection. The protein expression and secretion of the Xoo effectors XoAvrBs2 and XoAvrBs3 were assessed using dot blots, which enabled the monitoring of effector proteins at the early stages of the initial interaction, i.e., within 30 min of RLX treatment. The secretion of effectors was observed from 15 min after application of the pathogenic stimulus. In the P-activated proteome data, the expression of effector proteins was maintained at a similar level to that at 0 min; this may be attributed to the similar protein synthesis and secretion rates.

The effector genes are also dispersed across the genome, like the ion uptake genes (Figure S9). Interestingly, transposase genes are located close to the effector genes; these may aid the effector genes to transpose through the bacterial genome and plasmids. The expression of XoAvrBs2 was upregulated 5 min after RLX treatment, and its secretion was detected in the culture medium at 15 min. Although the cellular protein level was upregulated by approximately 20% in the proteome at 30 min, the dot blot showed an upregulation of 4-fold at 5 min. The secreted XoAvrBs2 exhibited a 16-fold increase at 120 min. In case of XoAvrBs3, the cellular protein level decreased by approximately 20% in the proteome at 60 min, whereas the dot blot revealed a 16-fold increase in XoAvrBs3 secretion at 120 min. However, one should take into consideration the fact that the experimental procedures for the dot blots and proteome analysis are different. For the dot blots, TAP-tagged *XoAvrBs2* and

348 *XoAvrBs3* genes were introduced into Xoo cells via a plasmid and TAP-tagged XoAvrBs2
349 and XoAvrBs3 proteins were quantitatively measured. In proteome analysis, XoAvrBs2 and
350 XoAvrBs3 proteins were expressed from the endogenous *XoAvrBs2* and *XoAvrBs3* genes in
351 the Xoo genome.

352 Gene expression involves sequential transcription and translation. In bacteria, with respect
353 to post-transcriptional and post-translational modification, mRNAs without a cap at 5' end
354 and a poly A tail at 3' end have a short half-life—as short as few minutes—and proteins
355 undergo only limited post-translational modifications. The limited post-translational
356 modifications in bacterial proteins imposes a pressure on a nascent protein from the ribosome
357 to take a functional form immediately. The present study revealed that genes related to cell
358 motility and inorganic ion uptake, and genes coding for effector molecules of Xoo are the
359 first to respond to the initial interactions with RLX, and play an essential role in the following
360 processes: (1) invasion of the Xoo cells into the damaged rice leaf tissues, (2) securing the
361 limited cofactors, and (3) modulating the immune responses of the host to favor pathogenesis.
362 This combined analysis of the time-resolved transcriptome and proteome of Xoo during the
363 initial interaction with rice tissues provides valuable insights into the pathogenic mechanism
364 of Xoo.
365

Materials and Methods

Bacterial strain and culture conditions

Xanthomonas oryzae pv. *oryzae* (Xoo) strain KACC10331, consisting of 4,941,439 nucleotides and 4,733 open reading frames, without any apparent autonomous plasmids, was obtained from the Korean Agricultural Collection Center (KACC) (Lee et al., 2005). The bacteria were cultured in nutrient broth (Difco, Detroit, MI, USA) or Yeast Glucose Cm Agar (YGC) (2.0% D-(+)-glucose, 2.0% $CaCO_3$, 1.0% yeast extract, and 1.5% agar) at 28°C.

Construction of expression vector and transformation of Xoo

The effector genes *XoAvrBs2* (*Xoo0168*) and *XoAvrBs3*—including the promoter region (from -149 and -750 bp to the start codon of the respective gene)—were amplified by PCR, and ligated into the pGEM®-T Easy Vector (Promega). The cloned sequences were verified and then digested with *Kpn*I and *Sac*I, and the products were ligated into the pHM1-XTAP-T_{gap} vector. The recombinant vectors were purified and introduced into Xoo strain KACC10331 by electroporation, using Gene Pulser II (Bio-Rad, Hercules, CA) with a 0.2 cm-gap cuvette at 2.5 kV cm^{-1}. Xoo cells were then diluted immediately with 1 mL Super Optimal Broth (SOC) medium and incubated at 28°C with agitation for 2 h. Cells were then recovered from the culture medium and plated on nutrient broth agar plates containing 50 μL mL^{-1} spectinomycin and incubated at 28°C for 4 d.

The transformants were cultured in 100 mL of nutrient broth up to the mid-exponential phase (A_{600} = 0.5). Cells were harvested by centrifuging 1 mL of the cell culture at 12,000 rpm and 4°C for 5 min. Harvested cells were washed once with phosphate-buffered saline (PBS) at pH 7.2, resuspended in 200 μL PBS, and then sonicated. Protein samples were serially diluted using 2 M urea or PBS in 96-well plates and then transferred to a

polyvinylidene difluoride membrane (PVDF; 0.2 μm, Bio-Rad) using a 96-well vacuum dot-blotter (Bio-Rad). The membrane was then washed thrice with PBS, blocked with 5% skim milk for 30 min, and subjected to a one-step immuno-affinity reaction using the rabbit peroxidase-anti-peroxidase soluble complex antibody (Sigma-Aldrich, St. Louis, USA). The membrane was developed, and bound antibodies were detected by chemiluminescence.

Treatment of rice leaf extract for proteome analysis

Oryza sativa L. cv. Milyang 23, a Xoo-susceptible rice cultivar, was used for performing proteome analysis. Rice plants were grown in a paddy field at Jeonju in South Korea (35°49'52.0"N 127°03'55.6"E) until panicle initiation (approximately 8 to 9 weeks). Forty clumped rice leaves were harvested and homogenized with liquid nitrogen using a mortar and pestle. One-gram aliquots of the resulting homogenate (RLX) were transferred to Eppendorf tubes and stored at -80°C. Xoo was cultured (100 mL) in nutrient broth up to the mid-exponential phase (A_{600} = 0.5) in a shaking incubator at 28°C and 200 rpm, and RLX (2 g) was then added to the culture medium. The culture (100 mL) was subjected to sequential filtration through a gauze, 40-μm nylon cell strainer (FALON, New York, USA), and 5-μm syringe filter (Sartorius, Germany) to remove RLX (0, 30, 60, 90, and 120 min after RLX addition). The filtered culture (100 mL) was centrifuged at 10,000 ×*g* and 4°C for 10 min. Duplicate samples were obtained for each time point from two independent experiments.

Sample preparation for proteome analysis

The harvested samples were lysed in a lysis buffer (9 M urea prepared in 20 mM HEPES (pH 7.5), supplemented with protease inhibitor cocktail (Complete mini, Roche) and phosphatase inhibitor (PhosSTOP, Sigma-Aldrich)) and sonicated on ice. The exact amount of proteins in

414 each sample was determined using the bicinchoninic acid assay. Protein integrity was
415 confirmed by SDS-PAGE and 200 µg of protein from each sample was used for analysis. The
416 disulfide bonds were reduced by treatment with 10 mM dithiothreitol for 1 h, and incubation
417 with 30 mM iodoacetamide (30 min in the dark) was performed to alkylate free sulfhydryl
418 functional groups. Samples were diluted with triethylammonium bicarbonate buffer (pH 8.0)
419 in a manner such that the final urea concentration was 1.5 M. Proteins were digested using
420 MS grade trypsin (Thermo Fisher Scientific) at a protein to enzyme ratio of 50:1 for 12 h at
421 37°C. The reaction was quenched by lowering the sample pH (<3) using trifluoroacetic acid.
422 The obtained peptides were desalted using a C18 spin column (Harvard) to remove salts and
423 other contaminants, and the purified peptides were dried. Then, they were isotopically labeled
424 using the 10-plex tandem mass tag (TMT, Thermo Fisher Scientific), as per the
425 manufacturer's protocol. The reaction was allowed to continue for 2 h at room temperature
426 and TMT-labeled samples were subsequently dried in a SpeedVac concentrator. Chemical
427 labeling with TMT was confirmed by liquid chromatography-tandem mass spectrometry (LC-
428 MS/MS), and the samples were pooled and fractionated using a basic reverse phase liquid
429 chromatography (RPLC) system. The pooled TMT-labeled peptide mixture was resuspended
430 in 10 mM ammonium formate and fractionated into 12 fractions using a C18 column (C_{18}, 5
431 µm pore size, 4.6 mm × 250 mm, XBridge, Waters). The fractionated peptides were dried and
432 stored at -80°C until LC-MS/MS analysis.
433
434 **LC-MS/MS and database search**
435 Each fractionated peptide sample was analyzed using an Orbitrap Fusion™ Lumos™
436 Tribrid™ Mass Spectrometer coupled with the Easy-nLC 1200 nano-flow liquid
437 chromatography system (Thermo Fisher Scientific). The dried peptides were reconstituted

using 0.1% formic acid and loaded on a C18 trap column. Peptides were resolved using a linear gradient solvent B (0.1% formic acid in 95% acetonitrile) and analyzed by high resolution mass spectrometry in the data-dependent acquisition mode. MS1 and MS2 were acquired for the precursor and the peptide fragmentation ions, respectively. MS1 scans were measured at a resolution of 120,000 and an *m/z* of 200. MS2 scans were acquired following the fragmentation of precursor ions by high-energy collisional dissociation (HCD) and were detected at a mass resolution of 50,000 and an *m/z* of 200. Dynamic exclusion was used to reduce redundant fragmentation of the same ions. The obtained mass spectrometry data were analyzed using the MaxQuant software (Tyanova et al., 2016a). Raw MS data were searched against the Xoo proteome in UniProt database. Carbamidomethylation of cysteine and 10-plex TMT modification of lysine and N-terminals were set as static modifications, whereas oxidation of methionine was set as a variable modification. False discovery rates at the levels of protein and peptide-spectrum matches were set at 0.01. The raw MS data and MaxQuant search results have been submitted to ProteomeXchange (project accession: PXD020135, reviewer access with username: reviewer34070@ebi.ac.uk and password: mzn76I1O).

Proteomic data analysis

The contaminant and reverse identified proteins were removed from the MaxQuant data. Proteins identified in both replicates were pooled for quantile normalization. The normalized values for the replicates were subjected to supervised hierarchical clustering and principal component analysis, using Perseus (Tyanova et al., 2016b), and the results were depicted in the form of a multi-scatter plot.

STRING map analysis

The list of proteins in the selected patterns from the hierarchical clusters was uploaded on the STRING database (https://string-db.org/) to analyze the protein interaction maps. The clusters of proteins in the blue and red classes, which show the similar time-resolved expression patterns, were analyzed, and the list including the gene names with the selected organism was inputted in the multiple proteins search setting. The number of nodes and edges were automatically calculated based on Xoo genes with a PPI enrichment p-value of 20.9E-10. Figures were downloaded in the PNG file format for visualization.

RNA-Seq and data analysis

In addition to the previously obtained RNA-Seq data for P-activated Xoo cells, RNA-Seq data at 90 and 120 min were obtained to correspond with the proteome data at these time points. RNA-Seq and data analysis were performed as previously described (Kim et al., 2016). Briefly, total RNA from samples was used to generate sequencing libraries, from which ribosomal RNA was removed using MICROBExpress Bacterial mRNA Enrichment Kit (Ambion, Austin, TX, USA), and enriched mRNA was prepared using Illumina TruSeq RNA Sample Preparation Kit (Illumina, San Diego, CA, USA). The RNA obtained after fragmentation was used to generate cDNA fragments, which were sequenced using Illumina Genome Analyzer IIx and mapped to the reference genome sequence (http://www.ncbi.nlm.nih.gov/nuccore/58579623?report=fasta) using CLC Genomics Workbench 4.0 (CLC bio, Aarhus, Denmark). Relative transcript abundance was calculated based on the number of reads per kilobase per million mapped sequence reads (RPKM).

Analysis of time-resolved continuous mRNA and protein expression

The RPKM values of the mRNAs in the transcriptome and TMT intensities of the proteins

in the proteome corresponded to the observed expression level of each gene at a given time point. To facilitate the comparison of gene expression levels, the observed expression level at each time point was converted to fold change in gene expression, by dividing the expression level at a given time point by the initial expression level (0 min) of the same gene. The fold change in the time-resolved expression levels of a given gene during the two hours following the RLX treatment was fitted to a curve and analyzed using non-linear regression by GraphPad Prism (version 3.02 for Windows, GraphPad Software, San Diego California USA, www.graphpad.com), and the continuous time-dependent changes in the mRNA and protein expression levels were determined using the fitted curve.

Analysis of the correspondence between mRNA and protein expression levels

For the accurate comparison of the mRNA and protein expression levels in P-activated Xoo cells, the expression levels were corrected by comparing with those in the control cells at each time point. The fold change in mRNA and protein expression in P-activated Xoo cells at a given time point was divided by that of the control cells at the same time point. For analyzing the correspondence between the mRNA and protein levels of each gene in the transcriptome and proteome, the resulting control-corrected fold change values of mRNAs were compared with those of the proteins for a given time point as the gene expression level of mRNAs and proteins.

Declarations

Compliance with ethics guidelines

Seunghwan Kim, Wooyoung Eric Jang, Min-Sik Kim, Jeong-Gu Kim, and Lin-Woo Kang declare that they have no conflict of interest. The authors declare no competing financial interests. This article does not contain any studies with human or animal subjects performed by the any of the authors.

Available data and material

The raw MS data and MaxQuant search results are available at ProteomeXchange (Project accession: PXD020135, Reviewer access with username: reviewer34070@ebi.ac.uk and password: mzn76I1O)

Funding

This work was undertaken in association with the Cooperative Research Program for Agriculture Science & Technology Development (Project No. PJ01327002020), Rural Development Administration, Republic of Korea.

Author Contributions

Investigation, Seunghwan Kim, Wooyoung Eric Jang, Min-Sik Kim, Jeong-Gu Kim, and Lin-Woo Kang; writing, Seunghwan Kim, Wooyoung Eric Jang, Min-Sik Kim, Jeong-Gu Kim, and Lin-Woo Kang; methodology, Seunghwan Kim, Wooyoung Eric Jang, Min-Sik Kim, Jeong-Gu Kim, and Lin-Woo Kang; funding acquisition, Jeong-Gu Kim, and Lin-Woo Kang; supervision, Min-Sik Kim, Jeong-Gu Kim, and Lin-Woo Kang. All authors have read

530 and agreed to the published version of the manuscript.

531

532 **Acknowledgments**

533 We are grateful to the staff members of the Cooperative Research Program for Agriculture
534 Science & Technology Development (Project No. PJ01327002020), Rural Development
535 Administration,

536

537 **Abbreviations**

538 Xoo, *Xanthomonas oryzae* pv. *oryzae*; RLX, rice leaf homogenate; KACC, Korean
539 Agricultural Collection Center; P-activated, Pathogenicity-activated; LC-MS/MS, liquid
540 chromatography-tandem mass spectrometry; COG, Clusters of Orthologous Groups; RPKM,
541 Reads per kilobase per million mapped reads

542

543

544 **References**

545

546 Garau, G., Garcia-Saez, I., Bebrone, C., Anne, C., Mercuri, P., Galleni, M., Frere, J.M., and
547 Dideberg, O. (2004). Update of the standard numbering scheme for class B beta-lactamases.
548 Antimicrobial agents and chemotherapy 48, 2347-2349.

549 Hershey, J.W.B., Sonenberg, N., and Mathews, M.B. (2019). Principles of Translational
550 Control. Cold Spring Harbor perspectives in biology 11.

551 Jackson, S.A. (2016). Rice: The First Crop Genome. Rice 9, 14.

552 Jones, J.D., and Dangl, J.L. (2006). The plant immune system. Nature 444, 323-329.

553 Kay, S., Hahn, S., Marois, E., Wieduwild, R., and Bonas, U. (2009). Detailed analysis of the
554 DNA recognition motifs of the Xanthomonas type III effectors AvrBs3 and
555 AvrBs3Deltarep16. Plant J 59, 859-871.

556 Kim, S., Cho, Y.J., Song, E.S., Lee, S.H., Kim, J.G., and Kang, L.W. (2016). Time-resolved
557 pathogenic gene expression analysis of the plant pathogen Xanthomonas oryzae pv. oryzae.
558 BMC genomics 17, 345.

559 Kim, S., Nguyen, T.D., Lee, J., Hong, M.K., Pham, T.V., Ahn, Y.J., Lee, B.M., Han, Y.S., Kim,
560 D.E., Kim, J.G., *et al.* (2013). Homologous expression and T3SS-dependent secretion of
561 TAP-tagged Xo2276 in Xanthomonas oryzae pv. oryzae induced by rice leaf extract and its
562 direct in vitro recognition of putative target DNA sequence. Journal of microbiology and
563 biotechnology 23, 22-28.

564 Kim, S.H., Lee, S.E., Hong, M.K., Song, N.H., Yoon, B., Viet, P., Ahn, Y.J., Lee, B.M., Jung,
565 J.W., Kim, K.P., *et al.* (2011). Homologous expression and quantitative analysis of T3SS-
566 dependent secretion of TAP-tagged XoAvrBs2 in Xanthomonas oryzae pv. oryzae induced by
567 rice leaf extract. Journal of microbiology and biotechnology 21, 679-685.

568 Lee, B.M., Park, Y.J., Park, D.S., Kang, H.W., Kim, J.G., Song, E.S., Park, I.C., Yoon, U.H.,
569 Hahn, J.H., Koo, B.S., *et al.* (2005). The genome sequence of Xanthomonas oryzae pathovar
570 oryzae KACC10331, the bacterial blight pathogen of rice. Nucleic acids research 33, 577-586.
571 Li, J.Y., Wang, J., and Zeigler, R.S. (2014). The 3,000 rice genomes project: new
572 opportunities and challenges for future rice research. GigaScience 3, 8.
573 Mew, T.W., Alvarez, A.M., Leach, J.E., and Swings, J. (1993). Focus on Bacterial-Blight of
574 Rice. Plant Disease 77, 5-12.
575 Mukherjee, S., and Kearns, D.B. (2014). The structure and regulation of flagella in Bacillus
576 subtilis. Annual review of genetics 48, 319-340.
577 Oliva, R., Ji, C., Atienza-Grande, G., Huguet-Tapia, J.C., Perez-Quintero, A., Li, T., Eom, J.S.,
578 Li, C., Nguyen, H., Liu, B., *et al.* (2019). Broad-spectrum resistance to bacterial blight in rice
579 using genome editing. Nature biotechnology 37, 1344-1350.
580 Quibod, I.L., Atieza-Grande, G., Oreiro, E.G., Palmos, D., Nguyen, M.H., Coronejo, S.T.,
581 Aung, E.E., Nugroho, C., Roman-Reyna, V., Burgos, M.R., *et al.* (2020). The Green
582 Revolution shaped the population structure of the rice pathogen Xanthomonas oryzae pv.
583 oryzae. The ISME journal 14, 492-505.
584 Schubert, O.T., Rost, H.L., Collins, B.C., Rosenberger, G., and Aebersold, R. (2017).
585 Quantitative proteomics: challenges and opportunities in basic and applied research. Nature
586 protocols 12, 1289-1294.
587 Tsuge, S., Furutani, A., and Ikawa, Y. (2014). Regulatory network of hrp gene expression in
588 Xanthomonas oryzae pv. oryzae. J Gen Plant Pathol 80, 303-313.
589 Tyanova, S., Temu, T., and Cox, J. (2016a). The MaxQuant computational platform for mass
590 spectrometry-based shotgun proteomics. Nature protocols 11, 2301-2319.
591 Tyanova, S., Temu, T., Sinitcyn, P., Carlson, A., Hein, M.Y., Geiger, T., Mann, M., and Cox, J.

(2016b). The Perseus computational platform for comprehensive analysis of (prote)omics data. Nature methods 13, 731-740.

Ullah, J.H., Walsh, T.R., Taylor, I.A., Emery, D.C., Verma, C.S., Gamblin, S.J., and Spencer, J. (1998). The crystal structure of the L1 metallo-beta-lactamase from Stenotrophomonas maltophilia at 1.7 A resolution. Journal of molecular biology 284, 125-136.

Scheme legend

Scheme 1. Schematic representation of the *in vitro* assay system and combined analysis of the time-resolved transcriptome and proteome using RNA-Seq and LC-MS/MS

606 ## Figure legends

607

608 **Figure 1. Time-supervised hierarchical clustering of duplicate pathogenicity-activated**
609 **proteome datasets.** The heatmap (left) of genes clustered based on the similarities in the
610 protein expression pattern over time is presented for duplicate samples of pathogenicity-
611 activated and control Xoo cells. Low to high expression is indicated by a change in color
612 from green to red. Selected cluster profile patterns (right) are presented for the down- (blue
613 box) and upregulated (red box) genes in the P-activated Xoo cells.

614

615 **Figure 2. Time-resolved protein expression patterns associated with the COG categories**.
616 Two functional categories of genes (COG) associated with the greatest changes in the protein
617 level are indicated by red boxes, nine functional COGs associated with moderate changes are
618 indicated by yellow boxes, and other nine functional COGs associated with minor changes in
619 the protein level are indicated by blue boxes. The inset for each functional COG indicates the
620 control (untreated cells). The Y-axis represents the fold change in the protein expression level
621 in comparison with that at 0 min, and the maximum value on the Y-axis was set as 3. The X-
622 axis indicates the time from 0 to 120 min. Each line indicates the protein expression level of a
623 gene. The protein expression level is represented as dotted (from 0 to 30 min) and solid (from
624 30 to 120 min) lines. Note that in contrast to the transcript data, the proteome data was not
625 available before 30 min (dotted part).

626

627 **Figure 3. Time-resolved mRNA and protein levels of genes associated with cell motility**
628 **and inorganic ion transport.** (A) Time-resolved expression of cell motility-related genes.
629 The mRNA expression levels from RNA-Seq are indicated by dashed red lines. The protein

630 expression levels from LC-MS/MS are indicated by black dashed (from 0 to 30 min) and
631 solid (from 30 to 120 min) lines. (B) Time-resolved expression of inorganic ion transport-
632 related genes. The mRNA expression levels from RNA-Seq and protein expression levels
633 from LC-MS/MS are indicated as in (A). The Y-axis represents the fold change.
634
635 **Figure 4. Gene clusters and time-resolved expression patterns of cell motility-related**
636 **genes.** (A) Gene clusters of flagellar biosynthesis-related genes (groups I-A and I-B) and
637 chemotaxis genes (group II). (B) Time-resolved mRNA and protein expression levels of
638 genes in groups I-A, I-B, and II. The down- and upregulation peaks are shown in green and
639 red, respectively. The yellow and grey ovals indicate unaltered and undetected expression
640 levels. The thin-bordered oval (at 5, 10, 15, and 45 min) for the proteome data is to ensure
641 consistency with the pictorial format of RNA-Seq data. The dotted arrows and ovals indicate
642 genes that are not directly related to flagellar biosynthesis and chemotaxis. Time is expressed
643 in min.
644
645 **Figure 5. Time-resolved mRNA and protein levels of iron transport-related genes.** (A)
646 Time-resolved mRNA (red) and protein (black) expression levels of *FecA* and *CirA* genes. (B)
647 Time-resolved mRNA (red) and protein (black) expression level of *IroN* genes. The Y-axis
648 represents $\log_2$(fold-change).
649
650 **Figure 6. Time-resolved mRNA and protein expression and protein secretion of genes**
651 **coding for effector molecules.** (A) The mRNA (red) and protein (black) expression levels of
652 *XoAvrBs2* gene (above) and dot blots of XoAvrBs2 protein in Xoo cells and culture medium
653 (below). (B) The mRNA (red) and protein (black) expression levels of *XoAvrBs3* gene (above)

654 and dot blots of XoAvrBs3 protein in Xoo cells and culture medium (below). NC, negative

655 control; PC, positive control

656

657

Supplementary data

Supplementary figure legends

Figure S1. Detailed analysis of the proteome data of pathogenicity-activated Xoo cells (A) Number of proteins identified from the high-resolution mass spectrometry-based quantitative proteomic analysis and (B) coverage percentage of the protein sequence of the identified proteins (median sequence coverage was ~24%). (C) Number of identified peptides and peptide-spectrum matches. (D) Quantile normalization box plot. (E) Multi-scatter plot for analyzing the correlations between samples.

Figure S2. Comparative analysis of the proteome of the samples (A) Quantile normalization box plot. The quantitative proteomic values were normalized using quantile normalization. (B) Multi-scatter plot for analyzing the correlation between samples. Pairwise comparisons of protein expression levels in all samples are presented as a multi-scatter plot. Pearson's correlation coefficients of 0.98-0.99 were obtained. (C) Principal component analysis of Xoo proteins revealed close relationships among the proteomes of all controls and changes in proteome concentrations upon RLX treatment.

Figure S3. Analysis and comparison of gene expression patterns in the datasets. The STRING maps (Benjamin-Hochberg at FDR 0.05) of selected cluster profile patterns with (A) down- (blue box) and (B) upregulated (red box) genes are shown.

Figure S4. Comparison of time-resolved mRNA and protein levels of cell motility-related genes. (A) Time-resolved mRNA levels of flagellar biosynthesis and chemotaxis-related genes for pathogenicity-activated Xoo cells. All genes in groups I-A, I-B, and II exhibited the lowest expression level at 5 min and the highest expression level at 30 min. (B) Time-resolved protein levels of flagellar biosynthesis and chemotaxis-related genes in pathogenicity-activated Xoo cells. Genes in groups I-A and I-B exhibited the highest expression level at 30 min, whereas those in group II exhibited the highest expression at 90 min.

Figure S5. Time-resolved mRNA and protein expression of iron uptake-related genes. Time-resolved mRNA (red) and protein (black) expression levels of iron uptake-related genes (A) *FecA* and (B) *CirA*. The Y-axis represents $\log_2$(fold change).

Figure S6. Gene cluster and time-resolved mRNA and protein expression levels of phosphate uptake-related genes. (A) Gene cluster of the phosphate uptake regulation genes (*OprO-PhoX-PstSCAB-PhoU*). (B) Time-resolved mRNA and protein expression levels of phosphate uptake-related genes *OprO*, *PhoX*, *PstSCAB*, and *PhoU*. The line colors correspond to those of the arrows in (A).

Figure S7. Gene clusters of cell motility-related genes in *E. coli* and Xoo and time-resolved mRNA and protein expressions of Xoo genes. Gene cluster of cell motility-related genes of (A) *E. coli* and (B) Xoo. (C) Time-resolved mRNA and protein expression of cell motility-related genes in Xoo. The cell motility-related genes in *E. coli* are classified as class I (red), II (yellow), III (blue), and II+III (green). The ortholog genes in Xoo are indicated

using the same color. For the proteome data, * indicates the expression peak at 30 min; **, between 30 and 90 min; ***, at 90 min. The Y-axis represents $\log_2$(fold change).

Figure S8. Gene clusters and time-resolved mRNA and protein expressions of iron uptake-related genes in Xoo. (A) Gene cluster of iron uptake-related genes, labelled in blue. (B) Time-resolved mRNA and protein expression levels of iron uptake genes. Low to high expression is indicated by a change in color from blue to red. Black cells indicate undetected expression.

Figure S9. Gene clusters and time-resolved mRNA and protein expressions of genes coding for effector molecules. (A) Gene cluster of effector genes, indicated in red. (B) Time-resolved mRNA and protein expressions of effector genes. Genes with available time-resolved proteomic data are labelled with *. Of the *avrXa7* and *avrXa3* genes, the mRNA levels of only the former were measured, indicated by +. Transposase genes are indicated in blue.

Supplementary Table legends

Table S1. The raw data of time-resolved expression levels of mRNAs and proteins in the transcriptome and proteome of P-activated and control Xoo cells. The RPKM values of mRNAs and TMT intensities of proteins were obtained from independent duplicated transcriptome and proteome analyses, respectively, representing the expression levels of mRNAs and proteins of each gene. The gene products that were not identified or measured are indicated by black cells.

Table S2. The list of selected genes with similar protein expression patterns in the time-supervised hierarchical clustering. The list of genes marked with blue (downregulated) and red (upregulated) rectangles in Figure 1, which presented distinct synchronized protein expression patterns. Of the 40 flagellum-related KEGG annotated genes, 21 were included in the list, of which 20 genes were upregulated and one gene was downregulated in the proteome.

Table S3. The time-resolved fold change in mRNAs and proteins in the transcriptome and proteome of P-activated and control Xoo cells. The fold change in gene expression was calculated by dividing the expression level of a gene at a given time point by that at 0 min. Cells are colored based on the expression level; low to high expression is indicated by a change in color from blue to red, with white indicating a fold change of 1.

744 **Table S4. The control-corrected time-resolved fold change in mRNAs and proteins in**
745 **the transcriptome and proteome.** For accurate comparison of the mRNA and protein
746 expression levels, the expression level of P-activated Xoo cells at each time point was
747 corrected by comparing with that of the control cells. The fold change value for the mRNA or
748 protein levels in P-activated Xoo cells was divided by that of the control cells at the same
749 time point. The number and percentage of genes exhibiting 20%, 50%, and 200% (2-fold) up-
750 and downregulation are indicated at the bottom of the table.

751

752 **Table S5. The number of consistently up- and downregulated genes during the entire**
753 **duration of 120 min.**

754

755 **Table S6. The list of proteins exhibiting 2-fold upregulation at 30 min in the duplicate**
756 **proteome datasets.**

757

758 **Table S7. The list of proteins downregulated by 50% at 30 min in the duplicate**
759 **proteome datasets.**

Scheme 1

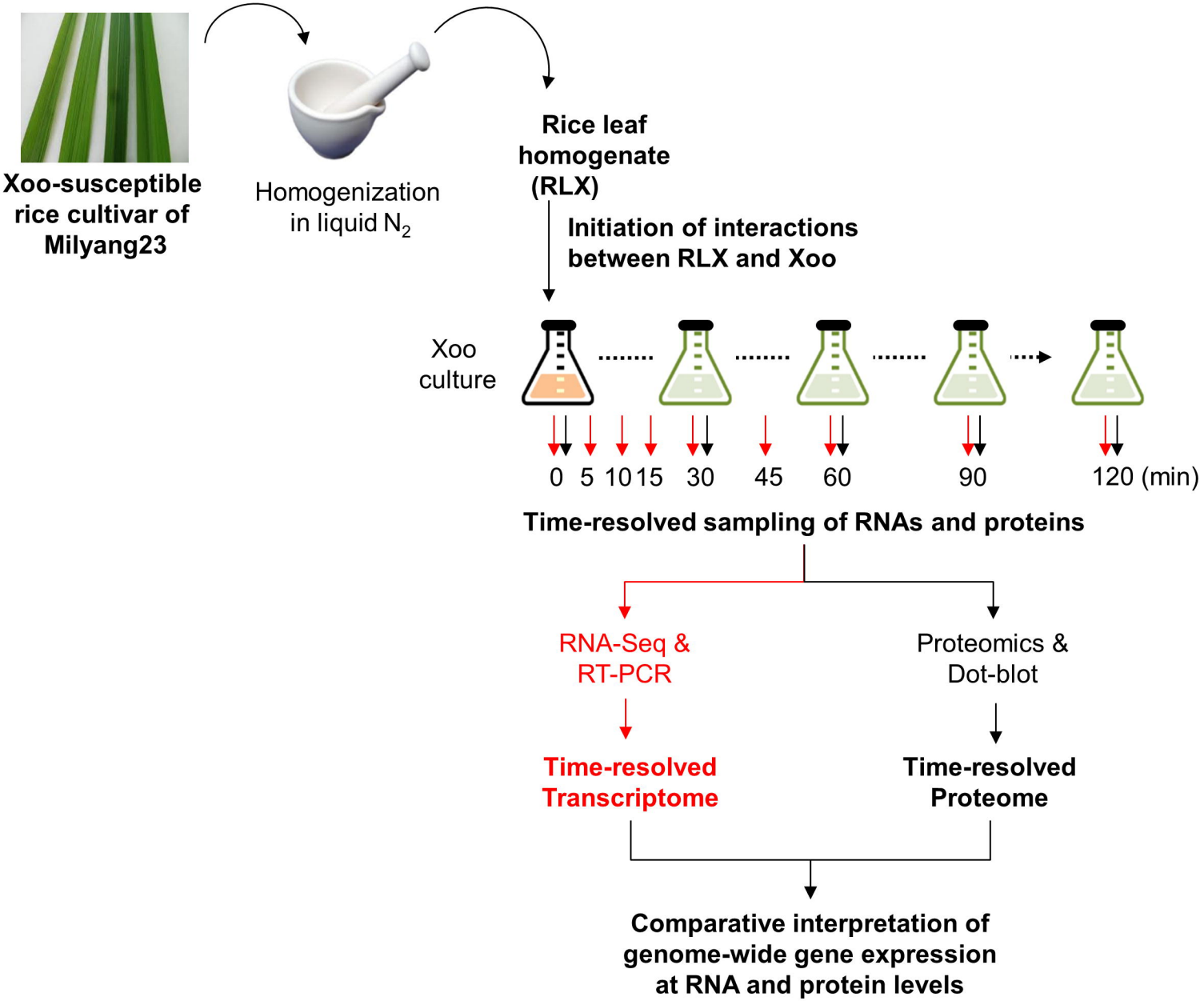
Xoo-susceptible rice cultivar of Milyang23
Homogenization in liquid N_2
Rice leaf homogenate (RLX)
Initiation of interactions between RLX and Xoo
Xoo culture
0 5 10 15 30 45 60 90 120 (min)
Time-resolved sampling of RNAs and proteins
RNA-Seq & RT-PCR
Proteomics & Dot-blot
Time-resolved Transcriptome
Time-resolved Proteome
Comparative interpretation of genome-wide gene expression at RNA and protein levels

Figure 1

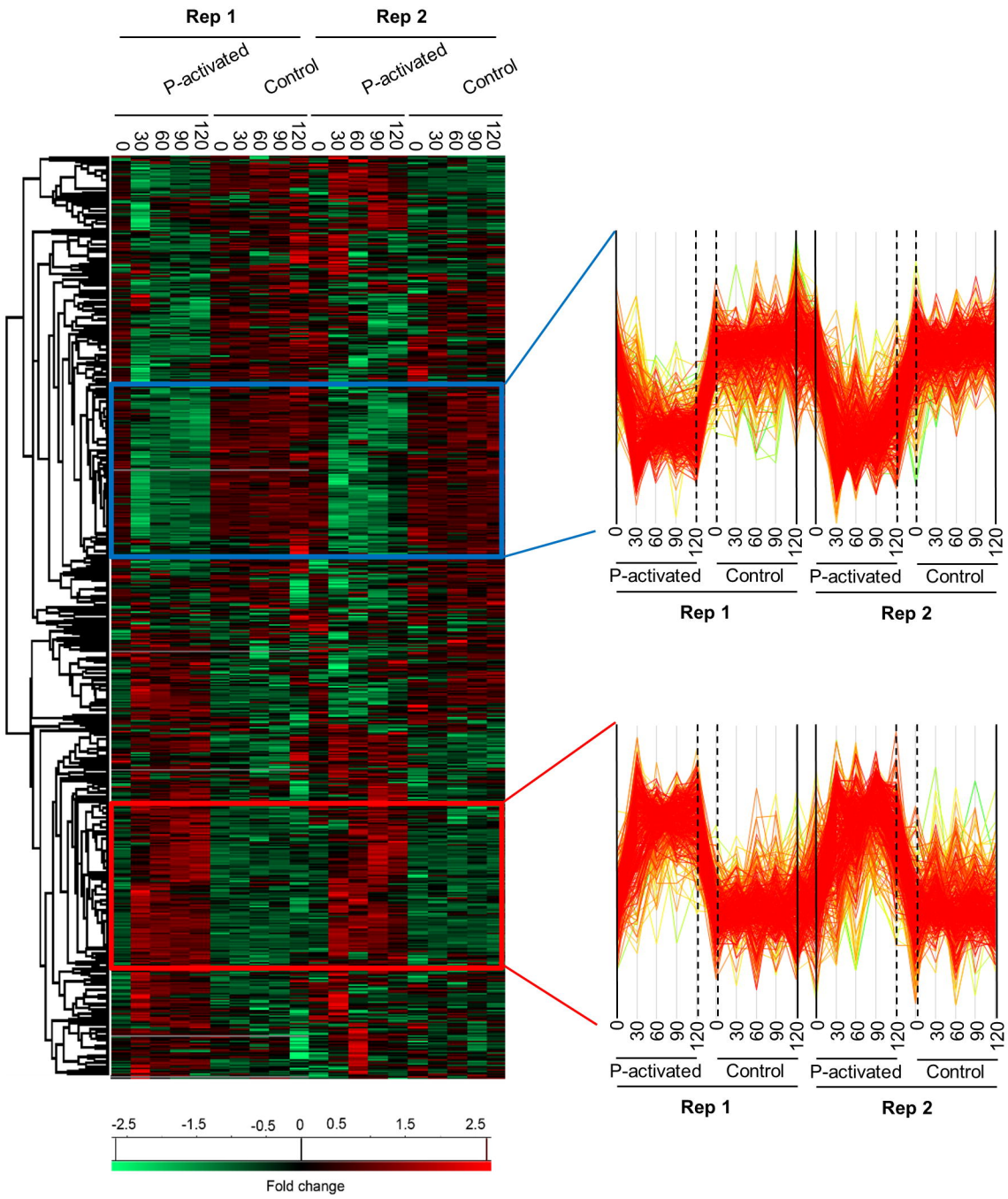
Rep 1
Rep 2
P-activated
Control
0
30
60
90
120
-2.5
-1.5
-0.5
0
0.5
1.5
2.5
Fold change

Figure 2

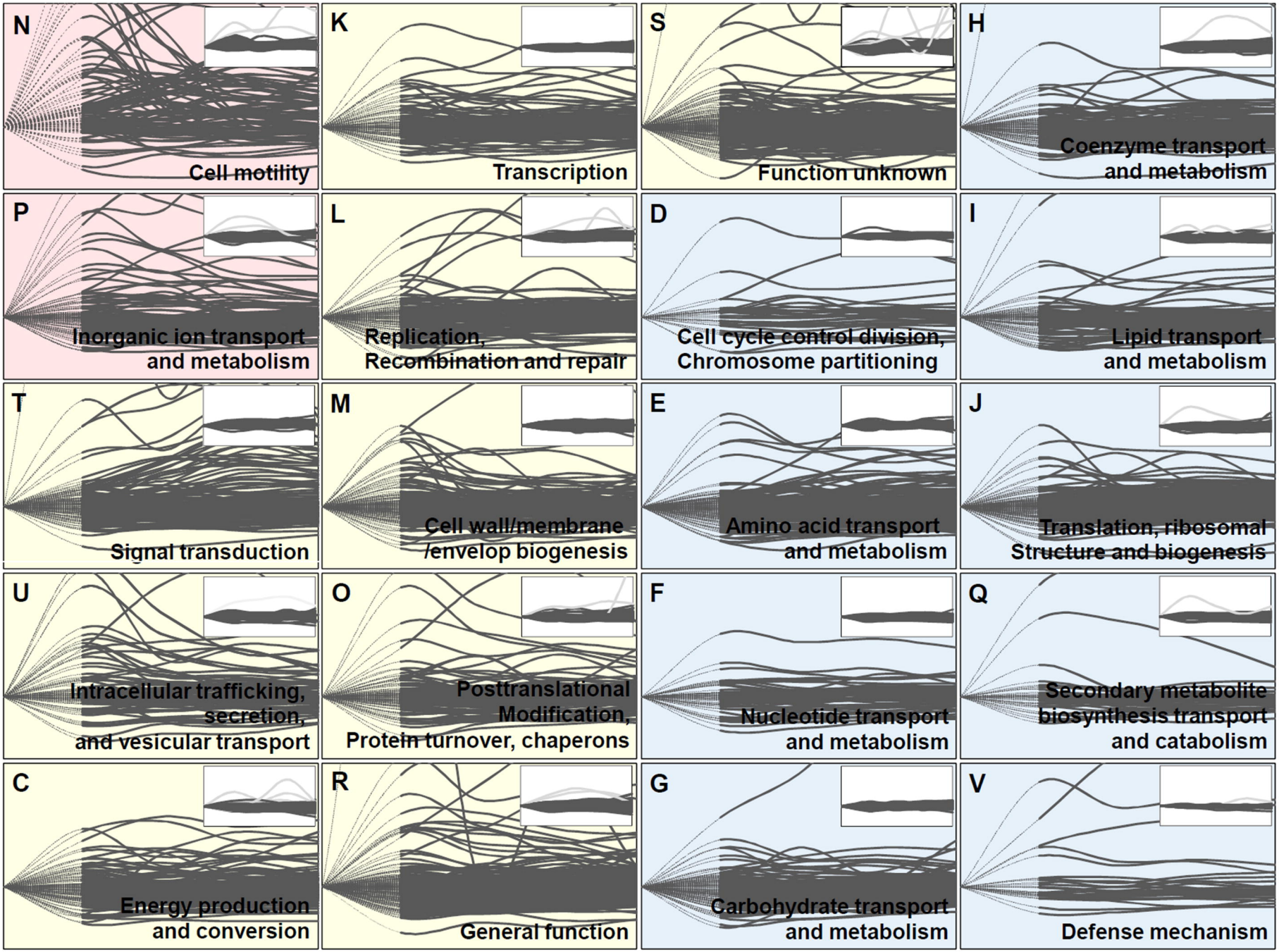
N
Cell motility
K
Transcription
S
Function unknown
H
Coenzyme transport
and metabolism
P
Inorganic ion transport
and metabolism
L
Replication,
Recombination and repair
D
Cell cycle control division,
Chromosome partitioning
I
Lipid transport
and metabolism
T
Signal transduction
M
Cell wall/membrane
/envelop biogenesis
E
Amino acid transport
and metabolism
J
Translation, ribosomal
Structure and biogenesis
U
Intracellular trafficking,
secretion,
and vesicular transport
O
Posttranslational
Modification,
Protein turnover, chaperons
F
Nucleotide transport
and metabolism
Q
Secondary metabolite
biosynthesis transport
and catabolism
C
Energy production
and conversion
R
General function
G
Carbohydrate transport
and metabolism
V
Defense mechanism

Figure 3

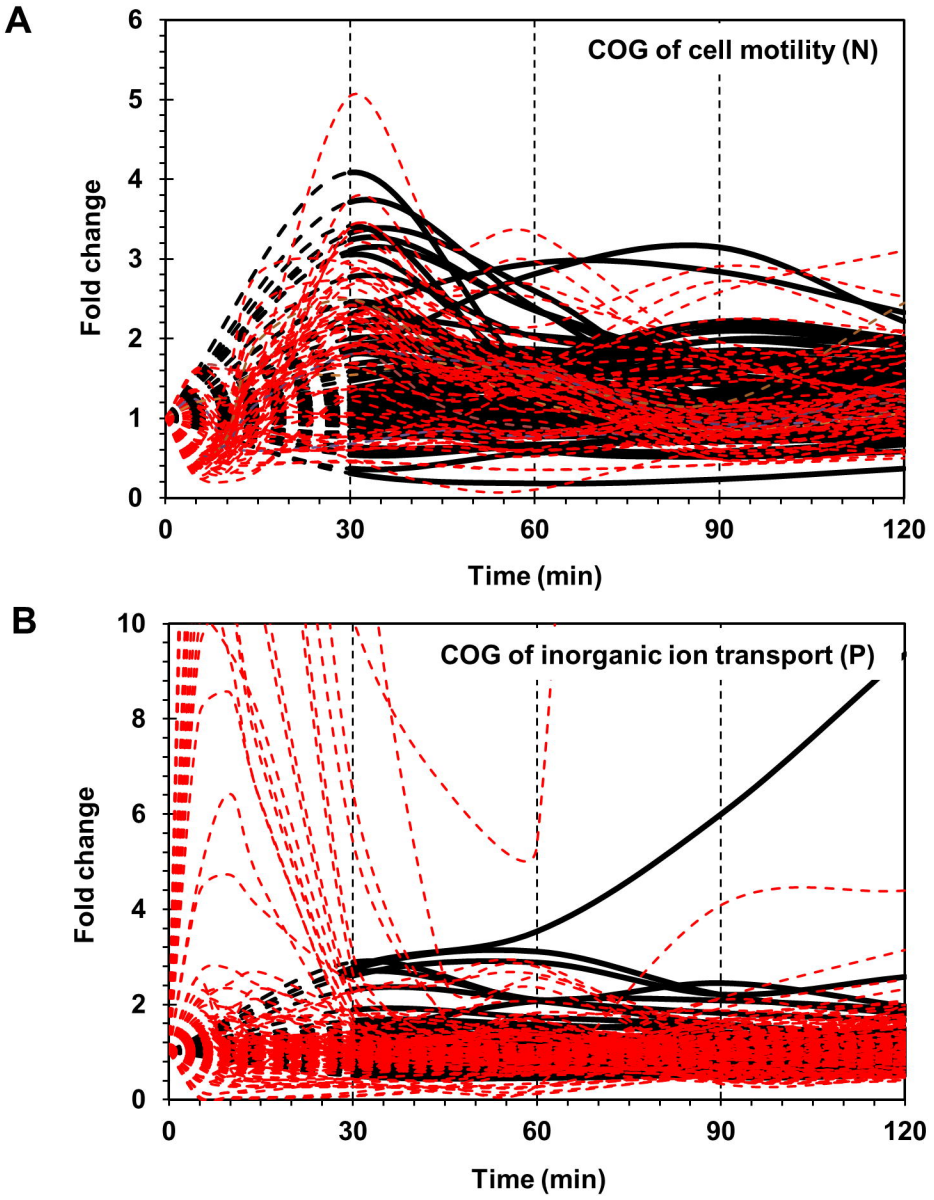
A
COG of cell motility (N)
Fold change
Time (min)
B
COG of inorganic ion transport (P)
Fold change
Time (min)

Figure 4

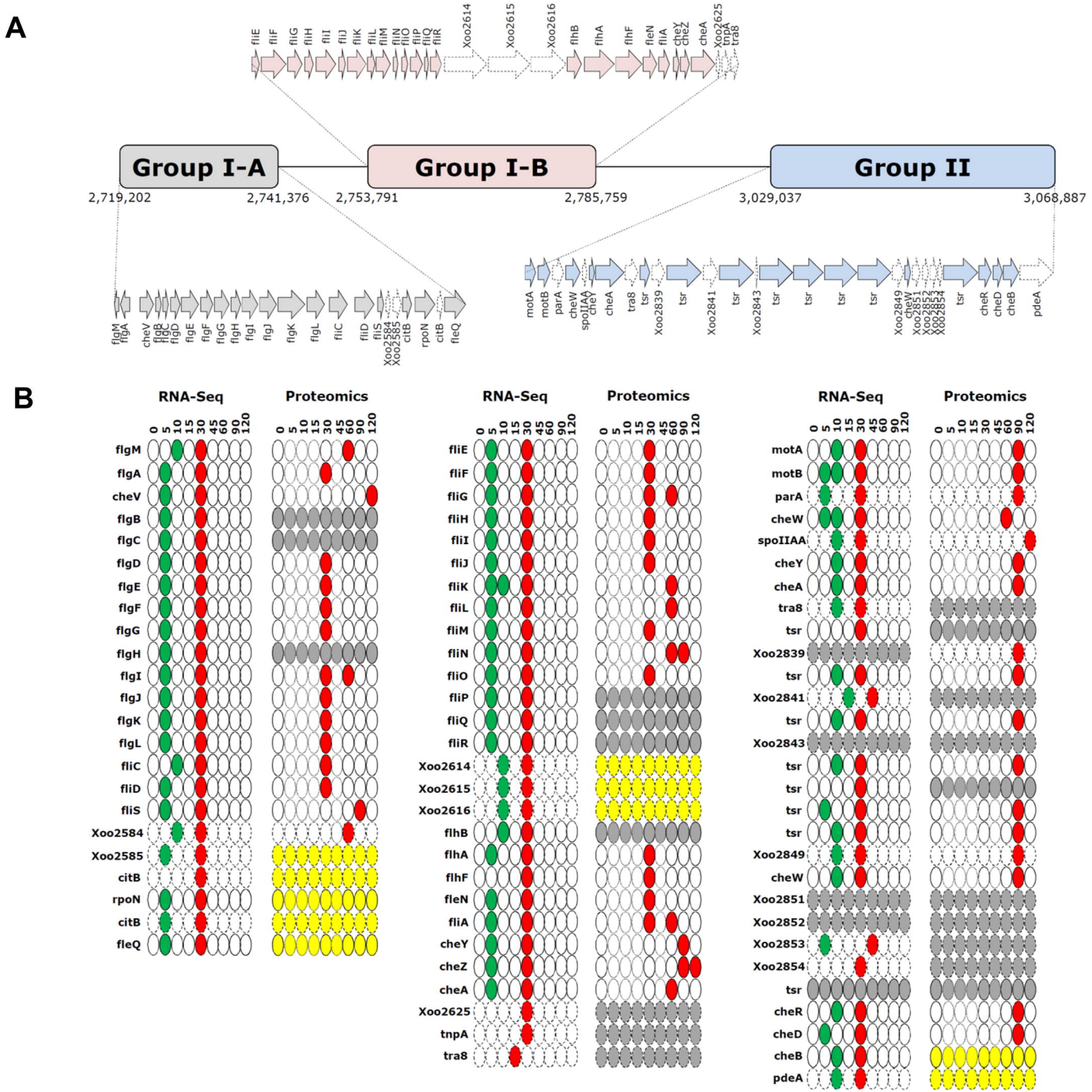
A
Group I-A
Group I-B
Group II
2,719,202
2,741,376
2,753,791
2,785,759
3,029,037
3,068,887
B
RNA-Seq
Proteomics
0 5 10 15 30 45 60 90 120
flgM
flgA
cheV
flgB
flgC
flgD
flgE
flgF
flgG
flgH
flgI
flgJ
flgK
flgL
fliC
fliD
fliS
Xoo2584
Xoo2585
citB
rpoN
citB
fleQ
fliE
fliF
fliG
fliH
fliI
fliJ
fliK
fliL
fliM
fliN
fliO
fliP
fliQ
fliR
Xoo2614
Xoo2615
Xoo2616
flhB
flhA
flhF
fleN
fliA
cheY
cheZ
cheA
Xoo2625
tnpA
tra8
motA
motB
parA
cheW
spoIIAA
cheY
cheA
tra8
tsr
Xoo2839
tsr
Xoo2841
tsr
Xoo2843
tsr
tsr
tsr
tsr
Xoo2849
cheW
Xoo2851
Xoo2852
Xoo2853
Xoo2854
tsr
cheR
cheD
cheB
pdeA

Figure 5

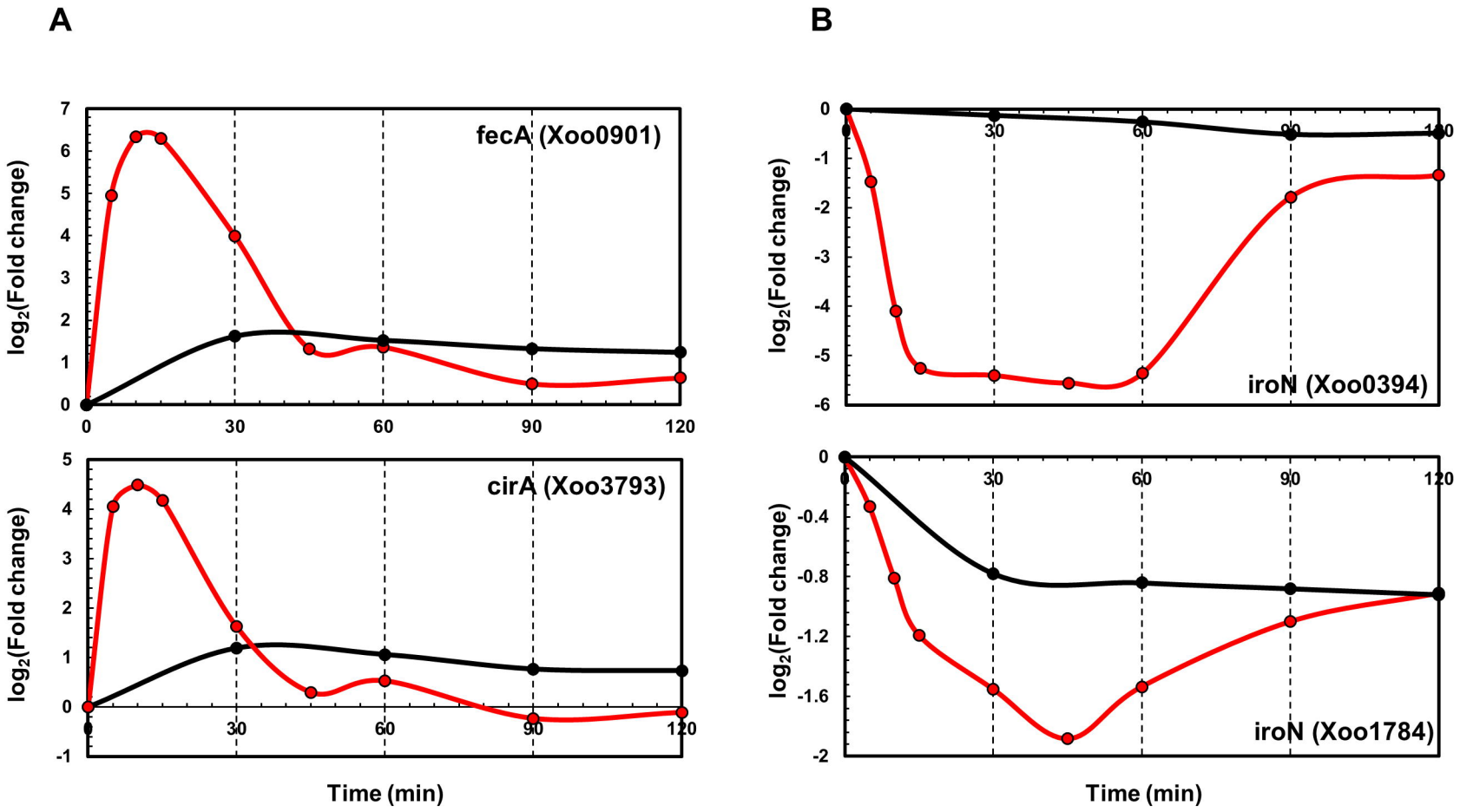
A
B
fecA (Xoo0901)
cirA (Xoo3793)
iroN (Xoo0394)
iroN (Xoo1784)
log2(Fold change)
Time (min)
0
30
60
90
120

Figure 6

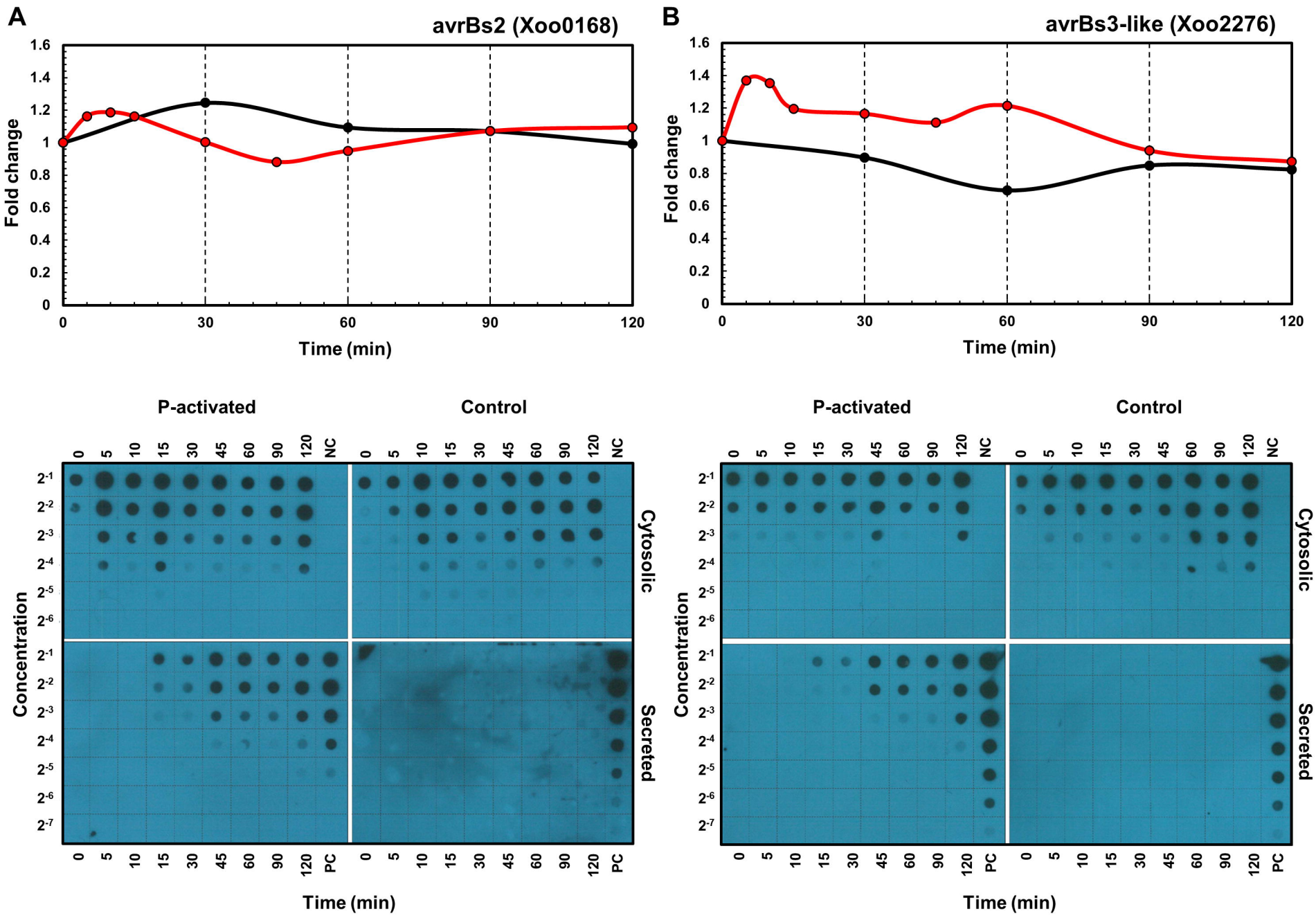
A
avrBs2 (Xoo0168)
Fold change
Time (min)
B
avrBs3-like (Xoo2276)
Fold change
Time (min)
P-activated
Control
Concentration
Cytosolic
Secreted
Time (min)
P-activated
Control
Concentration
Cytosolic
Secreted
Time (min)